ACS OMEGA

Open Access

http://pubs.acs.org/journal/acsodf

Article

Inspecting the Triazole Scaffold as Powerful Antifibril Agents against 2N4R Tau and α-Synuclein Aggregates

Ahmed A. Elbatrawy, Taiwo A. Ademoye, Heba Alnakhala, Arati Tripathi, Xiongwei Zhu, Germán Plascencia-Villa, George Perry, Ulf Dettmer, and Jessica S. Fortin*

Cite This: *ACS Omega* 2025, 10, 6721−6734

Read Online

ACCESS | Metrics & More | Article Recommendations | Supporting Information

ABSTRACT: Alzheimer's (AD) and Parkinson's (PD) disease are neurodegenerative disorders that are considered to be a significant global health challenge due to their increasing prevalence and profound impact on both individuals and society. These disorders are characterized by the progressive loss of neuronal function, leading to cognitive and motor impairments. A key pathological feature of AD and PD is the abnormal accumulation of misfolded proteins within the brain. In AD, amyloid-beta aggregates into plaques, while tau proteins form neurofibrillary tangles (NFTs). Parkinson's disease, on the other hand, is marked by the accumulation of α-synuclein (α-syn) in the form of Lewy bodies (LBs). These protein aggregates are involved in neuronal dysfunction and neurodegeneration, contributing to disease progression. Research efforts are increasingly focused on identifying small molecules that can simultaneously target multiple pathological processes, offering the potential to not only alleviate symptoms but also modify the progression of neurodegeneration. Herein, a novel group of triazole-based compounds was designed and synthesized to curtail the aggregation of α-syn and tau proteins, which are closely linked to the physiopathology of PD and AD, respectively. A thioflavin T (ThT) fluorescence assay was used to measure fibril formation and assess the antiaggregation effects of various compounds. To further validate these findings, transmission electron microscopy (TEM) was employed as a direct method to visualize the impact of these compounds on fibril morphology. Inhibition of oligomer formation was evaluated using photoinduced cross-linking of unmodified proteins (PICUP), enabling the detection of early protein aggregation events. During fibril formation assays, three compounds (**3e**, **4b**, **4d**) demonstrated superior inhibitory activity as assessed by ThT fluorescence and TEM imaging. Subsequent evaluations, which included tests for antioligomer, anti-inclusion, and disaggregation effects identified compound **4d** as the most promising candidate overall.

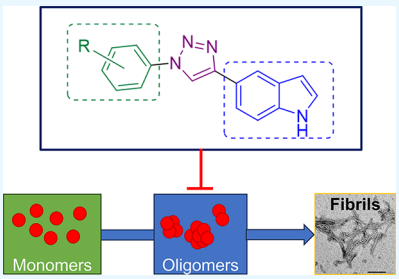

INTRODUCTION

Neurodegenerative diseases like Alzheimer's disease (AD) and Parkinson's disease (PD) are characterized by the abnormal accumulation of misfolded proteins.[1] These proteins, which are normally harmless, undergo structural changes that cause them to aggregate into compact insoluble fibrils.[2] As these intermediate species and fibrils build up in the brain, they disrupt normal cellular processes, leading to progressive neuronal damage and dysfunction.[2,3] The resulting impairment in brain activity manifests in the cognitive and motor symptoms associated with these devastating chronic diseases.[4] AD is characterized by distinct pathological features that disrupt normal brain function. Among these, amyloid plaques and neurofibrillary tangles (NFTs) are particularly significant.[5] Amyloid plaques consist of clusters of misfolded amyloid-beta proteins (predominantly fragments $A\beta_{1-40}$ and $A\beta_{1-42}$) that accumulate outside neurons, while NFTs are formed from tau proteins that have undergone abnormal modifications.[6,7] These NFTs develop inside neurons and disrupt their structural integrity. However, misfolded tau proteins have also been detected in the synaptic cleft.[8] Together, these plaques and NFTs interfere with the brain's ability to transmit signals effectively, leading to the gradual decline in cognitive abilities associated with AD. Although amyloid-beta plaques develop early in the disease, research shows that cognitive decline is more strongly correlated with the spread of NFTs throughout the brain.[9,10] NFTs arise from the accumulation of tau proteins, which normally play a critical role in stabilizing microtubules within neurons. However, when tau proteins become hyperphosphorylated, they lose their ability to bind to microtubules and get detached, leading to the formation of NFTs and contributing to neuronal dysfunction and cell death.[10,11] When tau proteins detach from microtubules, they become prone to interacting with other tau molecules.[12] These interactions lead to the formation of small oligomers, which gradually assemble into larger structures with a β-sheet configuration. These aggregates grow in size and complexity,

Received: September 12, 2024
Revised: January 22, 2025
Accepted: January 29, 2025
Published: February 12, 2025

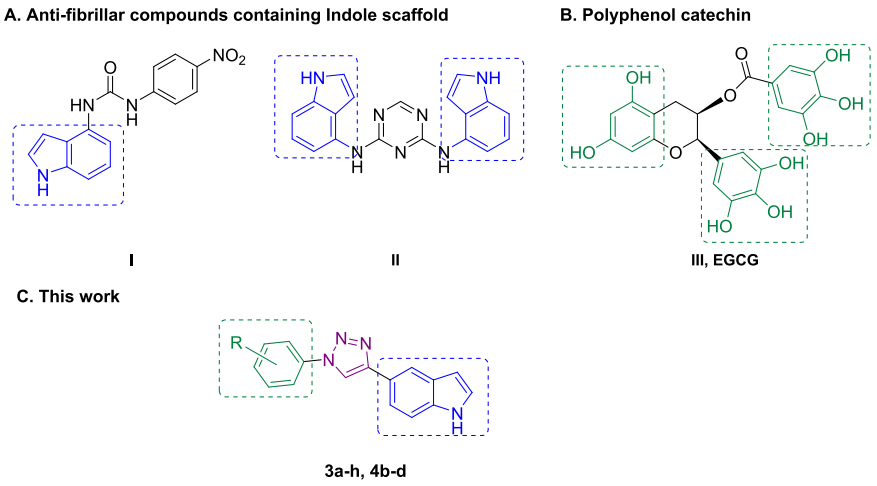

Figure 1. Design of the synthesized compounds as dual antifibrillar agents. (A) Antifibrillar agents I[24] and II[22] containing indole scaffold previously published from Dr. Fortin laboratory; (B) Polyphenol catechin (−)-epi-gallocatechin-3-gallate (EGCG); and (C) designed compounds in this study.

Scheme 1. Synthetic Procedure for the Target Compounds 3a−h and 4b−d[a]

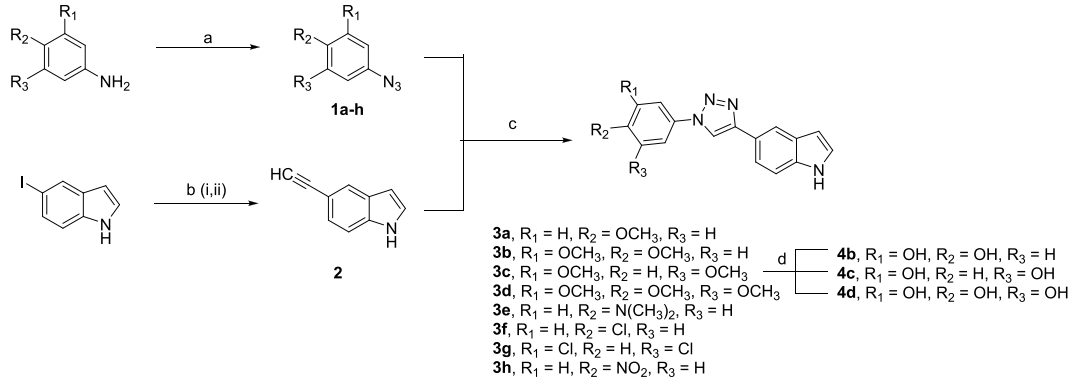

[a]Reagents and conditions: (a) $NaNO_2$, NaN_3, HCl:H_2O (1:1), 0-5°C, 3 h, 85-100% yield; (b) (i), $PdCl_2(PPh_3)_2$, CuI, TEA, DMF, r.t., 5−8 h; (ii) aq. NaOH, MeOH, r.t., 1 h, 72% yield (over the two steps); (c) Na ascorbate, $CuSO_4.5H_2O$, THF:H_2O (1:1), r.t., 71-91% yield; (d) BBr_3, DCM, 0°C, overnight, 8-12% yield.

eventually forming tau fibrils that develop into NFTs.[13,14] NFTs first appear in the transentorhinal cortex, a region in the temporal lobe, before spreading to other critical areas of the brain such as the hippocampus and, eventually, the neocortex.[15] This spread of NFTs is a key driver of the cognitive decline seen in AD, as they progressively damage the brain's neuronal networks.[16]

PD prominently features the accumulation of misfolded alpha-synuclein (α-syn) known as Lewy bodies (LBs) within neuronal cells.[17] Central to this pathologic effect is α-syn, which normally exists as a soluble, largely monomeric entity in the brain. Under certain conditions, α-syn undergoes various post-translational modifications, such as phosphorylation, acetylation, glycation, and ubiquitination, which are, at least in part, disease-associated. Moreover, the transition from an unstructured form to one that is more folded and richer in alpha-helices has been proposed to be an early event in disease-relevant α-syn dyshomeostasis.[18] This and other conformational changes are thought to facilitate the protein's aggregation into dimers and oligomers. Over time, such oligomers combine into larger, insoluble aggregates that constitute LBs.[19] The accumulation of these structures likely disrupts normal neuronal function by impairing neurotransmitter signaling and triggering pathways that contribute to neuronal cell death.[20]

Current therapeutic approaches for AD and PD primarily focus on managing symptoms rather than targeting the underlying pathophysiological mechanisms. This symptomatic treatment often provides only short-term benefits and does not significantly enhance long-term health outcomes. Herein, polyphenolic triazole-linked indole compounds were designed and synthesized as multitarget agents, with the aim of inhibiting the aggregation processes of α-syn and tau proteins. Among them, the trihydroxy derivative, compound **4d**, showed a highly significant antifibrillar activity as depicted by decreasing the thioflavin-T (ThT) fluorescence to lower than 5% against α-syn and to ∼50% toward tau 4R isoforms. Transmission electron microscope (TEM) analyses of **4d** revealed powerful inhibitory activities against dense fibrils of both proteins which were consistent with their ThT assay results. In addition, **4d** was able to inhibit the early stage oligomer formation of α-syn protein in a dose-dependent manner. **4d** reduced tau 0N4R oligomers at high micromolar concentration. Finally, **4d** reduced the α-syn inclusion formation in M17D neuroblastoma reporter cells.

https://doi.org/10.1021/acsomega.4c08385
ACS Omega 2025, 10, 6721−6734

Table 1. Antifibrillary Activity of the Newly Synthesized Triazoles (100 μM) on α-Syn Fibril Formation (2 μM)[a]

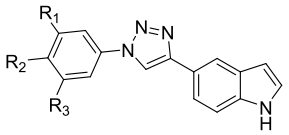

3a-h, 4b-d

Compound ID	R_1	R_2	R_3	α-synThT %	Compound ID	R_1	R_2	R_3	α-synThT%
3a	H	OCH_3	H	>100	**3g**	Cl	H	Cl	>100
3b	OCH_3	OCH_3	H	>100	**3h**	H	NO_2	H	>100
3c	OCH_3	H	OCH_3	>100	**4b**	OH	OH	H	14.3 ± 6.3
3d	OCH_3	OCH_3	OCH_3	>100	**4c**	OH	H	OH	77.1 ± 2.2
3e	H	$N(CH_3)_2$	H	11.8 ± 3.7	**4d**	OH	OH	OH	3.9 ± 1.7
3f	H	Cl	H	54.0 ± 1.5					

[a]The average of three triplicate results was taken from the maximum thioflavin T (ThT) fluorescence intensity at the plateau phase of the kinetics of aggregation. The average of the maximum of fluorescence is expressed as a percentage with the standard error of the mean (SEM). Control consisted of 0.25% DMSO. ThT results over 100% refer to the incapacity at reducing α-syn fibril formation.

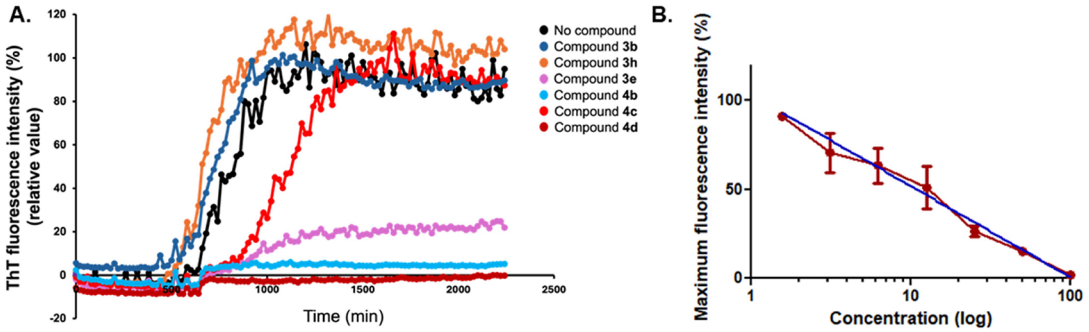

Figure 2. Kinetics of α-syn formation with several triazole based-compound and dose−response of the lead, compound **4d**. (A) Thioflavin T (ThT) kinetic curves illustrating the fibrillation process of α-syn (2 μM) with the thiazole compounds (100 μM). The control condition included only the vehicle (0.25% DMSO). For each experimental condition, triplicate measurements were taken at ten consecutive time points during the plateau phase of the fibrillation process. (B) Monomeric α-syn (6 μM) was subjected to variable concentrations of compound **4d** to achieve the dose−response curve. Using Prism GraphPad, a nonlinear regression was applied in the semilog graph and the following equation was obtained $Y = 103.3-51.33 *\log(X)$ with sum of squares of 13.30. The trend line is indicated with a blue color. The dose−response curve exhibited a clear, dose-dependent linear relationship, indicating the compound's potency in modulating the biological response across the tested concentration range of 6.25, 12.5, 25, 50, and 100 μM at 37 h incubation.

RESULTS AND DISCUSSION

Design of the Prepared Compounds. Our research group has identified and elaborated the indole scaffold in several significantly active antifibrillar compounds against different prone-to-aggregate proteins (compounds **I** and **II**, Figure 1A).[21−24] Thanks to their strong hydrogen-bonding capabilities, electron-donating characteristics, and stability, the triazoles can interact with multiple biological targets in neurodegeneration,[25,26] such as inhibiting the formation of amyloid plaques and preventing neurotoxicity.[27] Therefore, triazoles are believed to be promising candidates for preventing or reducing the formation of toxic protein aggregates associated with neurodegenerative diseases. The polyphenolic green tea catechin, (−)-epi-gallocatechin-3-gallate (EGCG), revealed powerful antifibrillar and antioligomeric properties toward α-syn and tau deposits (Figure 1B).[28−32] Thus, the prepared compounds were destined to have the indole moiety connected to polyphenols using the triazole linker (Figure 1C). In addition, we evaluated the importance of the polyphenolic groups by exchanging them with electron-rich or electron-deficient groups such as methoxy and dimethylamino groups, or nitro and chloro substituents, respectively.

Chemistry. The synthesis of the designed compounds is outlined in Scheme 1. Briefly, different azides (**1a−h**) were simply prepared by diazotization of the corresponding anilines with sodium nitrite and hydrochloric acid followed by reaction with sodium azide. The commercially available 5-iodo-1*H*-indole reacted with ethynyltrimethyl silane in the presence of a palladium catalyst and base. The crude product was then subjected to hydrolysis with sodium hydroxide to get the 5-ethynyl derivative, **2**, in a good yield. The targeted compounds **3a−h** were successfully achieved by Hüisgen Cu(I)-mediated [3 + 2] click cycloaddition reaction between the substituted aromatic azides (**1a−h**) and the terminal alkyne (**2**). Finally, demethylation of the di- or trimethoxy groups was performed by reacting **3b−d** with boron tribromide yielding the corresponding di- or triphenols, **4b−d**, respectively.

Biophysical Evaluation. *Thioflavin T (ThT), or Thioflavin S (ThS) Fluorescence Assays.* To assess the ability of our compounds to inhibit α-syn aggregation, we monitored the fibril formation using Thioflavin T (ThT) fluorescence intensity over time. ThT is known to bind to β-sheet structures present in amyloid-like fibrils, which restricts the rotation of the molecule and increases its fluorescence signal.[33] In our study, we incubated each compound (100 μM) with α-syn monomers (2 μM) for ≥27 h (Table 1). The results were

https://doi.org/10.1021/acsomega.4c08385
ACS Omega 2025, 10, 6721−6734

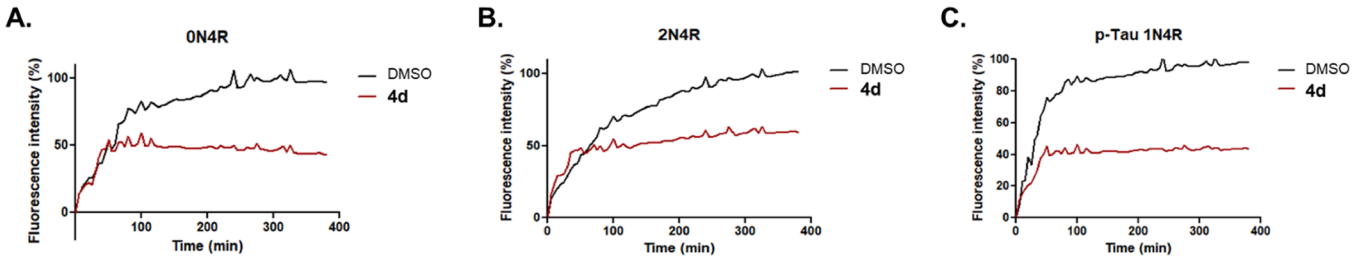

Figure 3. Lead **4d**, a polyphenol triazole-based compound, reduced the aggregation of tau nonphosphorylated and phosphorylated 4R isoform by about 50%. The ThS fluorescence curves of **4d** illustrate the aggregation kinetics of (A) tau 0N4R (6 μM), (B) tau 2N4R (12 μM), and (C) p-tau 1N4R (6 μM) in PBS-treated with chelex beads. The solution was supplemented with 150 μM heparin, 5 mM dithiothreitol (DTT), 40 μM ThS, and 10 mg/mL arachidonic acid in order to induce the aggregation. The control condition contained 0.25% DMSO, while compound **4d** was tested at a concentration of 100 μM. The data represented by each curve are an average of three independent replicates.

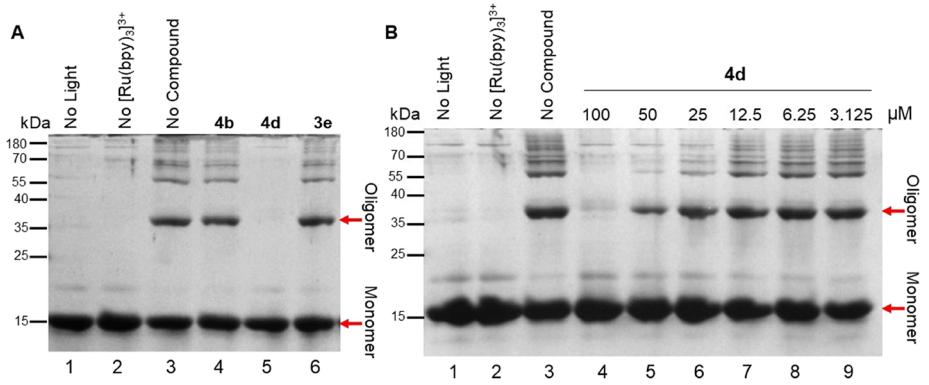

Lane	Pixel density	% reduction
1	135	-
2	142	-
3	14015	0
4	12532	11
5	168	99
6	13088	7

Lane	Pixel density	% reduction
1	206	-
2	94	-
3	17800	0
4	1477	92
5	8605	52
6	12984	27
7	14881	16
8	16223	9
9	17369	2

Figure 4. Lead compound **4d** exhibited a concentration-dependent inhibitory effect on α-syn oligomerization. (A) Compound **4d** effectively prevented the formation of α-syn oligomers induced by tris(2,2'-bipyridyl)dichlororuthenium(II) hexahydrate($[Ru(bpy)_3]^{3+}$) and ammonium persulfate under brief light exposure (1 s) in the PICUP cross-linking assay. For this assay, α-syn (30 μM) was cross-linked in the presence of 100 μM of the lead compound. The samples prepared were not incubated for any substantial time prior PICUP experiments. In the control sample, which contained 0.25% DMSO without the test compound, higher molecular weight α-syn oligomers were clearly observed on Coomassie blue-stained polyacrylamide gels. In contrast, additional control samples that were either not exposed to light or lacked the cross-linking agent ($[Ru(bpy)_3]^{3+}$) did not show any cross-linked products. (B) Monomeric α-syn (30 μM) was subjected to varying concentrations of the lead compound followed by PICUP cross-linking assay. Samples were loaded on a 16% polyacrylamide SDS-Page gel electrophoresis and stained with Coomassie blue to reveal the cross-linking products. The concentration-dependent α-syn antioligomer effect of lead compound **4d** was confirmed. As the concentration of compound **4d** decreased, there was a corresponding increase in the intensity of the high molecular weight bands (corresponding to oligomer). DMSO (0.25%) was used as a control, showing no significant impact on oligomer formation. The percentage of oligomer reduction is calculated by dividing the oligomer pixel density located between 35 and 40 kDa (most likely corresponding to dimer or mixture of higher order polymers) of the lane with compound treatment by the oligomer pixel density of the control lane (without the compound) and then multiplied by 100. The resulting value is then subtracted from 100 to determine the reduction.

reported as the average of the maximum fluorescence intensity at the plateau phase where the fibrils are mature, and the disaggregation and elongation are in equilibrium. The percentages are compared to evaluate the compound effects on fibril formation. Throughout the incubation period, fluorescence was measured every 20 min to monitor changes in intensity. The introduction of compounds **3a**, **3b**, **3c**, **3d**, **3g**, and **3h** led to an increase in fluorescence. Conversely, compounds **3e**, **4b**, and **4d** reduced fluorescence intensity by ≥80% compared to the control, where monomeric α-syn was incubated with DMSO at 0.25%. This suggests that these specific compounds have the potential to inhibit α-syn fibril formation. The maximum ThT fluorescence intensities in percentage resulting from α-syn incubated with compounds **3e**, **4b**, and **4d** were 11.8 ± 3.7, 14.3 ± 6.3, and 3.9 ± 1.7%, respectively (Table 1). Interestingly, the triazoles with electron-rich substituents such as polyphenol or phenyl-dimethylamino groups resulted in a drastic reduction of ThT fluorescence. One triazole with polyphenol compound, **4c**, and one with the chloride (electron-deficient group) substituted aromatic, **3f**, resulted in a moderate reduction of ThT fluorescence intensity of ∼23 and ∼46%, respectively (Table 1).

https://doi.org/10.1021/acsomega.4c08385
ACS Omega 2025, 10, 6721−6734

The kinetics of fibril formation of the best triazole compounds are presented in Figure 2A. Compounds **3a, 3c–d,** and **3f–g** were excluded from the kinetic analysis curves because their ThT fluorescence values significantly exceeded those of the control. Compounds **3a**, **3b**, **3c**, **3d**, **3g**, and **3h**, resulted in ThT data that were over 100% (Table 1). These compounds were not able to reduce the fibril formation. Compounds **3b** and **3h** were included as negative control (Figure 2A). They most likely have increased the formation of fibrils. Following the initial ThT assay, a dose–response curve was generated for compound **4d** (Figure 2B). To validate the inhibition of α-syn aggregation, the ThT assay was repeated with two concentrations of protein (2 and 6 μM). Compound **4d** was tested at an incremental increase of concentrations. The dose–response graph is nonlinear (without a logarithmic scale). With Prism software, the X axis was converted in a logarithmic scale, and a nonlinear correlation was applied. Nonlinear regression to an appropriate nonlinear model created a curve that appeared straight on these axes. With this type of correlation, the following equation was obtained $Y = 103.3-51.33 *\log(X)$ with sum of squares of 13.30. The trend line (Semilog line -- X is log, Y is linear) is in blue (Figure 2B). The result shows the varying α-syn antiaggregation effect of compound **4d** in the dose–response profile.

Additionally, **4d** was tested at 100 μM resulting in an approximate molar ratio protein:compound of 1:8 (12 μM tau 2N4R) and 1:16 (6 μM for tau 0N4R and p-tau 1N4R). The antiaggregation effect of the best lead (i.e., **4d**) on the 4R tau isoforms (0N4R, 2N4R) and the hyperphosphorylated tau isoform 1N4R was assessed using thioflavin S (ThS) (Figure 3). The kinetics of fibril formation of the nonphosphorylated and phosphorylated tau isoform 4R demonstrated a reduction of approximately 50% in fibril formation, indicating the potential efficacy of compound **4d** in inhibiting the aggregation of tau proteins.

Photo-Induced Cross-Linking of Unmodified Protein (PICUP) Assay. The formation of oligomers from amyloid-like fibril forming proteins is a crucial event in the development of protein-misfolding diseases.[34] These oligomers are generated at the early stage of the kinetics of aggregation. They form pore-like structures capable to disturb the integrity of lipid membranes of organelles and cells. The stress response generated by these oligomers may trigger apoptosis. These intermediate species participate to the generation of further aggregated protein. Therefore, these oligomers are known for their cytotoxic properties and play a crucial role in the spread of further misfolded protein and the progression of the disease.[34,35] In our earlier research, we employed the Photoinduced Cross-linking of Unmodified Proteins (PICUP) assay to generate stable α-syn and tau oligomers.[21−23] This technique provided a means to test the effectiveness of various compounds in inhibiting or mitigating the formation of these pathological oligomers. Within the experimental condition used herein, the PICUP assays allow for the formation of oligomer at 35–40 kDa for α-syn and >180 kDa for tau 0N4R. The proteins are treated with different compound and subjected readily (without any incubation time) to the cross-linking reagents and incandescent light exposure for the generation of the oligomer formation.

The impact of our compounds was explored on the oligomerization of α-syn and tau 0N4R isoform. Initially, we evaluated the three best triazole-based compounds at inhibiting α-syn fibril formation (i.e., **3e**, **4b**, and **4d**) at a concentration of 100 μM against 30 μM of α-syn to identify their potential antioligomerization effects (Figure 4A). Among the tested compounds, compound **4d** demonstrated the highest efficacy in preventing α-syn oligomerization while **4b** and **3e** had little effect as indicated by the percentage of reduction of oligomer formation. The most effective antioligomer compound was further analyzed to determine its dose–response relationship with regard to inhibiting α-syn oligomer formation. Compound **4d** was tested at variable concentrations ranging from ~3 to 100 μM. Compound **4d** at 100 μM reduced 99–92% and at 50 μM reduced 52% of α-syn oligomers located between 35 and 40 kDa, most likely populated by dimer or trimer, or mixture of oligomers. The dose–response studies of the lead compound indicated concentration-dependent inhibitory effects on α-syn oligomerization as shown in Figure 4B.

Our prior experience suggests that the reduction of tau aggregation, particularly the oligomer formation, is more challenging in comparison with the reduction of α-syn aggregation. Taking this difficulty into consideration, the tau antioligomer effect was assessed using the isoform 0N4R (at 6 μM) and a higher concentration of the lead compound **4d** (Figure 5). The high molecular weight bands resulting from the cross-linking reaction were located above the 180 kDa benchmark. Pixel density measurements of each band were executed. A reduction of 35, 46, and 72% of the tau 0N4R oligomer formation was obtained with 100, 200, and 300 μM of compound **4d**, respectively, in comparison with the condition without compound. The monomeric band was more abundant with the treated tau 0N4R with 100, 200, and 300 μM of compound **4d**.

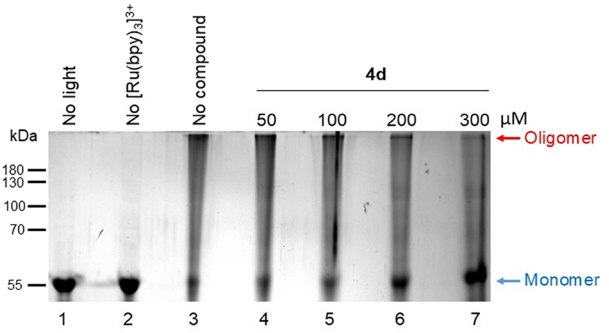

Lower bands (monomer)

Lane	Pixel density	% appearance
1	18998	107
2	16348	93
3	2603	15
4	2719	15
5	3310	19
6	5894	33
7	8274	47

Upper bands (oligomer)

Lane	Pixel density	% appearance
1	252	-
2	257	-
3	9096	100
4	9023	99
5	5984	65
6	5068	54
7	2696	28

Figure 5. Lead compound **4d** exhibited a tau 0N4R antioligomer effect at high micromolar concentration. The tau 0N4R high molecular weight band corresponding to oligomer was observed above 180 kDa after loading samples subjected to the PICUP cross-linking assay. Tau (6 μM) in the presence of and ammonium persulfate was cross-linked under light exposure at a duration of 15 s. The samples were not incubated with the compounds prior the light exposure. The percentages of oligomer or monomer appearance were calculated by dividing the pixel density of the lane with compound treatment by the pixel density of the control lane (without the compound) and then multiplied by 100.

https://doi.org/10.1021/acsomega.4c08385
ACS Omega 2025, 10, 6721−6734

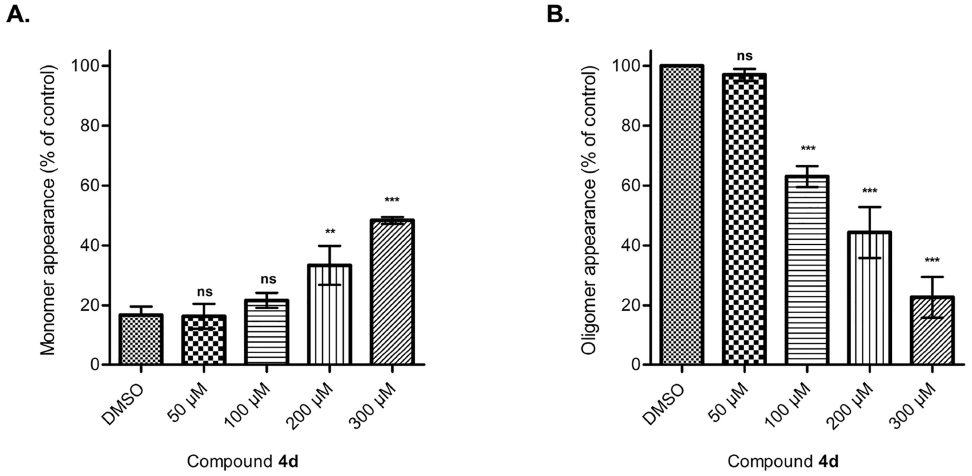

Figure 6. Compound **4d** inhibits tau 0N4R oligomer formation and preserves monomeric species. (A) Percentage of residual tau 0N4R monomer remaining after treatment with compound **4d**. The dose−response effect was evaluated using the PICUP cross-linking assay at different compound concentrations (50, 100, 200, and 300 μM). (B) Percentage of tau 0N4R oligomers detected after treatment with compound **4d** at varying concentrations (50, 100, 200, and 300 μM). The results demonstrated a reduction in oligomer levels and increase monomer levels with increasing compound concentration. Average and SEM from three independent experiments were plotted in histograms. Original data are presented in Figures S45−S47. The statistical significance of differences between compound-treated samples and the control (DMSO, no compound treatment) was assessed using Dunnett's post hoc test with $p < 0.01$ as the significant level.

Pixels of each tau monomeric band and oligomeric band were measured with ImageJ from three different experiments. The gels from these three independent experiments are presented in Figures S45−S47. The average from the percentage of appearance of tau monomers and oligomers were plotted in histograms presented in Figure 6. At a concentration of 300 μM of compound **4d**, the reduction of about 65% of tau oligomer was obtained and preservation of about 45% of tau monomer was observed.

Transmission Electron Microscope (TEM) Analysis. To explore the influence of compound **4d** on the ultrastructural morphology of α-syn and tau 2N4R fibrils, we conducted TEM analyses. Figure 7 presents TEM images of α-syn fibrils collected after the ThT assay from a 96-well plate. The images depict fibrils formed under untreated conditions and those exposed to compound **4d** at 12.5 and 100 μM. The untreated control, which included 0.25% DMSO, displayed numerous fibrils, and the same was observed with the compound treatment at 12.5 μM. In contrast, the sample treated with 100 μM compound **4d** showed a different morphology that corresponds to proto-fibril. Those proto-fibrils were rarely encountered on the grids and the treatment demonstrated a significant decrease in proto-fibril density as demonstrated by the measurement of the surface area of 1.3 ± 0.5 μm^2 ($N = 5$) by ImageJ (Figure 8) in comparison with the control which resulted in 24.4 ± 5.5 μm^2 ($N = 3$), corroborating the inhibitory effect observed in the ThT assay.

In the TEM images of tau 2N4R (Figure 9), compound **4d** demonstrated the ability to prevent the formation of fibrils. Tau 2N4R was coincubated with either compound **4d** (100 μM), EGCG (100 μM) or DMSO (0.25%; 'CTRL') for 5 days prior to imaging. In this experiment, EGCG was used as a positive control due to its proven ability to inhibit the aggregation of misfolded proteins, such as tau fibrils.[29,31] The known response of EGCG provides a reference for comparison, allowing us to assess the degree of inhibition of tau 2N4R aggregation under treatment with our best compound. The sample treated with compound **4d** showed a significant decrease in fibril formation, highlighting the compound's enhanced inhibitory effect compared to the control condition (0.25% DMSO).

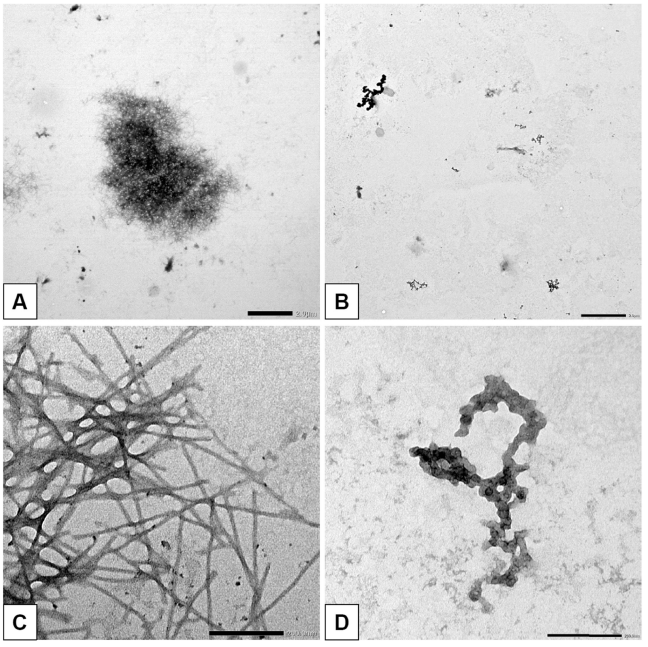

Figure 7. Transmission electron microscopy (TEM) evaluation demonstrated that compound **4d** significantly inhibited α-syn fibril formation. α-Syn (6 μM) was incubated with 0.25% DMSO as the control (CTRL) (A, C) and treated with compound **4d** at concentration of 100 μM (B, D). After an incubation period of approximately 37 h, the samples were visualized using TEM. At low magnification (2500), dense mats of fibrils were observed with the control (DMSO) and small clumps were rarely encountered with the compound **4d**. At high magnification (40k), many fibrils were observed with the control (DMSO) and the treatment with compound **4d** resulted in rare proto-fibrils (bedded chain pattern). Scale bars in the images A and B represent 2 μm. Scale bars in the images C and D represent 200 nm.

https://doi.org/10.1021/acsomega.4c08385
ACS Omega 2025, 10, 6721−6734

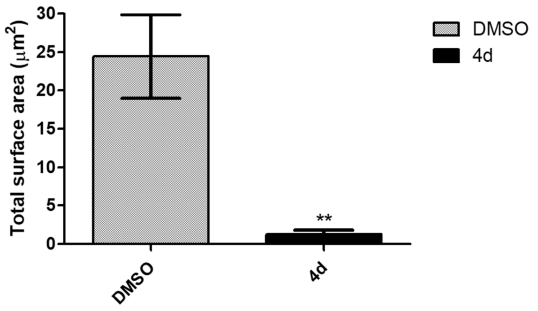

Figure 8. Areas covered by α-syn fibrils and proto-fibrils from the experiment presented in Figure 7. The surface covered by fibrils were measured using TEM images at a magnification of 2500. Areas covered by α-syn fibrils and proto-fibrils were compared between DMSO and compound **4d**. ImageJ software was used to set up the scale, adjust threshold, and measure area in μm^2. Different sample preparations deposited on copper grids were used for the analysis and one representative picture was selected from each grid. Three images obtained from independent grids for the control (DMSO) were quantified. Five images from three independent grids were analyzed for the treatment with compound **4d**. $^{**}p < 0.001$ by unpaired t test, two-tailed p value.

Disaggregation Assay Using Amyloid-Beta Plaques Extracted from AD Brains. The conceptualization of the triazole-based compounds in this study was designed using the indole moiety (as utilized in our prior work)[21−24] and polyphenol moiety of EGCG. EGCG is known to disaggregate preformed α-syn and amyloid-beta (Aβ) fibrils.[28,36] Next, we investigated the disaggregation effect of compound **4d** because EGCG demonstrated disaggregation effects on several amyloid-like fibrils. The antiaggregation and disaggregation effects of compound **4d** were explored first with the recombinant amyloid beta 1−40 (Aβ_{1-40}). Aβ_{1-40} was pretreated only 1 h with 1,1,1,3,3,3-Hexafluoro-2-propanol (HFIP) and exhibited some aggregates at the beginning of the kinetics (Figure 10A). Aβ_{1-40} peptide was used at a concentration of 21 μM and treated with ranging concentration of each compound. The ThT curves obtained from EGCG and **4d** demonstrated the disaggregation and antiaggregation effect on the A$\beta_{1\text{-}40}$ fragment, resulting in low percentage of ThT (Figure 10A). The maximum fluorescence intensity in percentage were obtained from the last ten data at the end of the kinetics for each compound (Figure 10B,C). Compound **4d** and EGCG reduced the percentage of ThT fluorescence significantly.

From our prior experience, general inhibitors of aggregation often exhibit disaggregation activity on mature fibrils. We aimed to confirm the disaggregation effect of compound **4d**. The recombinant amyloid-like fibrils are slightly different than the amyloid-like fibrils isolated from disease patients. For this reason, the disaggregation effect of lead compound **4d** was assessed using Aβ plaques extracted from AD patients (ex vivo). Protein concentration was measured with the Lowry method, and samples corresponded to 0.593 ± 0.095 mg/mL. The Aβ plaque-rich solution was incubated with 50 μM of compound **4d** or EGCG. The nontreated control showed fibril-dense rich plaques (Figure 11). In comparison to the control (0.25% DMSO), the materials resulting from compound **4d** were less defined and fibril-sparce. EGCG treatment resulted in less defined extravesicular-like materials supporting the reversal of fibrils into presumably nontoxic species.

α-Synuclein Inclusion-Forming Neuroblastoma Cell Experiment. To assess how different compounds influence α-syn inclusion formation, "3KY19" M17D neuroblastoma cells were used.[37] These cells are engineered to express the αS3K::YFP fusion protein when subjected to doxycycline (dox) treatment. The setup was designed to mimic the pathology of familial PD, particularly focusing on the E46K mutation. To intensify the disease model, a triple mutation (E35K + E46K + E61K), known as αS3K, was incorporated that readily forms distinct round inclusions in the cytoplasm of cultured cells. This model serves as an effective tool for studying disease mechanisms and evaluating the anti-inclusion effect of various compounds.[21−24,38,39] The cells were treated with different concentrations of compounds **4b** and **4d**, starting 24 h after they were plated. **4b** was selected because of its lack of antioligomer effect. Compound **4b** had a slightly weaker antifibrillar effect in comparison with compound **4d**. Inclusion formation was initiated 48 h after plating via the addition of doxycycline to initiate the expression of the fusion protein. Inclusion formation was quantified at 96 h to determine the dose-dependent effects of compounds **4b** and **4d**. Compound **4d** markedly decreased α-syn inclusion formation at concentrations of 2.5, 5, 10, 20, and 40 μM, with the most notable reduction observed at 40 μM (Figure 12A,C). Conversely, compound **4b** did not reduce α-syn inclusion levels. The cell confluence was unaffected during the treatment period (Figure 12B).

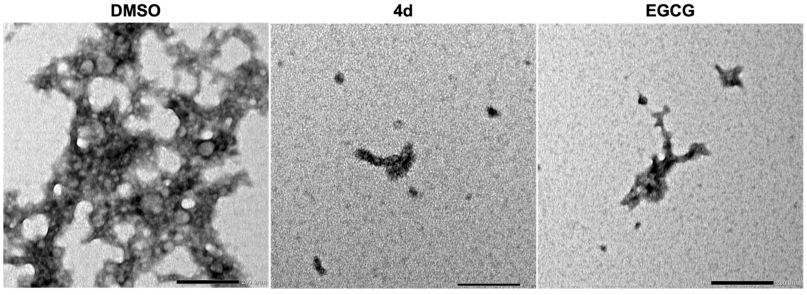

Figure 9. Lead compound **4d** reduced the formation of tau 2N4R fibril formation as validated by transmission electron microscopy (TEM). TEM was employed to directly assess the effect of compound **4d** on the monomeric tau isoform 2N4R (tested at 12 μM). Samples were treated with either DMSO (0.25%) as a control or 100 μM of compound **4d** and incubated at 37 °C for 5 days. Scale bars correspond to 200 nm, with images captured at 40k magnification.

https://doi.org/10.1021/acsomega.4c08385
ACS Omega 2025, 10, 6721−6734

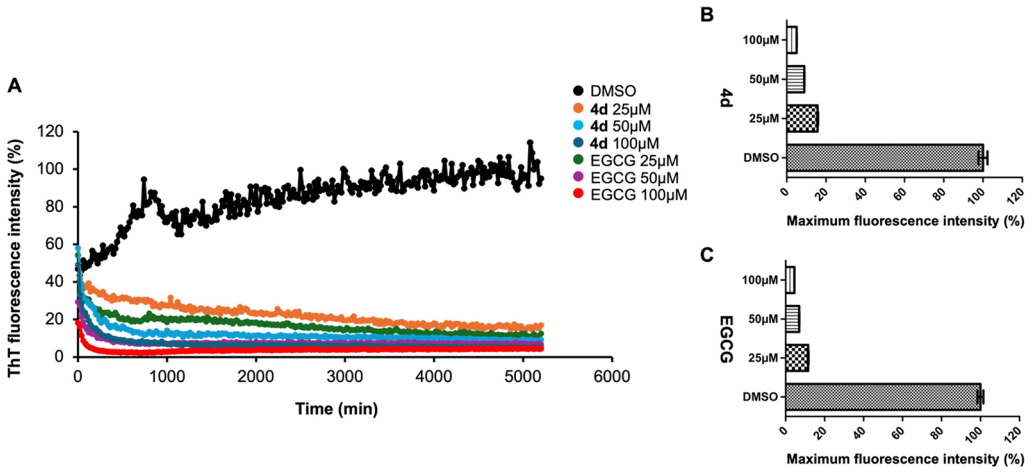

Figure 10. Compound **4d** and EGCG disaggregate and prevent the formation of amyloid beta1−40 ($A\beta_{1-40}$) fibrils. (A) Thioflavin T fibril formation kinetics of 21 μM $A\beta_{1-40}$ was assessed in the presence of compound **4d** and EGCG at 25, 50, and 100 μM concentrations. ThT was used at a final concentration of 40 μM. (B) Maximum fluorescence intensity in percentage was obtained at the end of the kinetics (approximately at 86 h) to evaluate the effects of compound **4d** on $A\beta_{1-40}$ fibril formation in comparison with the control (0.25% DMSO). (C) Similarly the maximum fluorescence intensity in percentage were plotted for the EGCG treatment and the control (0.25% DMSO). For those two histograms, compound **4d** and EGCG treatment were statistically significantly different compared to the control (0.25% DMSO) at $p < 0.001$ using the one-way ANOVA, Dunnet's posthoc test.

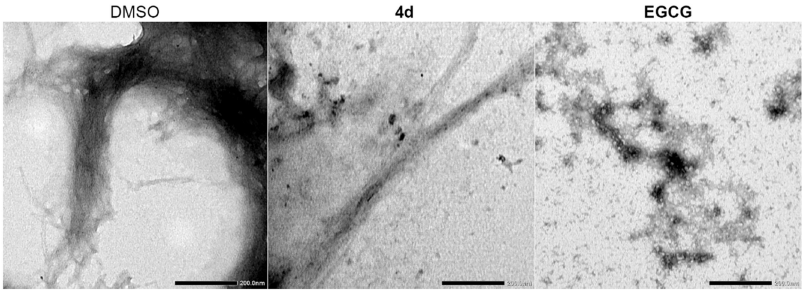

Figure 11. Compound **4d** exhibited a moderate disaggregation effect in comparison to EGCG, as confirmed by transmission electron microscopy (TEM). The disaggregation effect of compound **4d** was compared to EGCG. EGCG resulted non fibrillar structures. The nontreated control presented dense plaques comprised of fibrils. Amyloid beta (0.593 ± 0.095 mg/mL) solutions obtained from the brain of an AD patient were incubated with DMSO (0.25%; referred to as "CTRL"); compound **4d** (at 50 μM); or EGCG (at 50 μM) for 5 days at 37 °C before preparation of Formvar/carbon supported copper grids and direct visualization by TEM. Pictures were acquired at 40K. The scale bars correspond to 200 nm.

CONCLUSIONS

In summary, phenolic indoles connected to a triazole linker were designed and synthesized to prevent α-syn and tau aggregation. Using a ThT assay, the triphenolic derivative **4d** induced a significant loss in the fluorescence intensity of about 95% with α-syn aggregates and approximately 40 to 60% with tau (0N4R, 2N4R) and p-tau (1N4R). Moreover, **4d** exhibited an α-syn and tau (0N4R) antioligomer activity at high micromolar concentration employing the PICUP assay. The TEM analyses validated the ability of **4b** to reduce the fibril density of both α-syn and 2N4R. In addition, the cell-permeable compound **4d** robustly prevented the formation of α-syn inclusion in a cell-based assay. Compound **4d** demonstrated the ability to disaggregate $A\beta$ fibrils. Further structural modification is ongoing to exclusively target early stage oligomers.

METHODS

Chemistry. *General Characterizations.* All reagents and solvents were commercially available (Sigma-Aldrich, St. Louis, MO; Thermo Scientific (formerly Alfa Aesar), Waltham, MA; Matrix Scientific, Columbia, SC; Ambeed, Arlington Hts, IL) and were used without further purification. Thin-layer chromatography (TLC) was used to monitor the reaction progress. Organic solutions were dried over anhydrous magnesium sulfate. The solvents were evaporated on a Büchi rotavapor R-100 equipped with a Büchi V-100 vacuum controller. The nuclear magnetic resonance (NMR) spectra were recorded on a Bruker spectrometer at a frequency of 500 MHz for ^{1}H and at 126 MHz for ^{13}C. Proton chemical shifts are reported in parts per million (ppm) with the solvent reference relative to tetramethyl silane (TMS) employed as the internal standard (CDCl3, δ 7.26; DMSO-d6 δ 2.54). The multiplicities of NMR signals are designated as s (singlet), d (doublet), dd (double doublet), t (triplet), q (quartet), m (multiplet, for unresolved lines). High-resolution mass spectrometry (HRMS) of the compounds was carried out on Advion Mass Spectrometer (Advion Expression CMS) at the Analytical Mass Spectrometry Facility within the Purdue Institute for Drug Discovery. Uncorrected melting points (m.p.) were scored using an electrothermal apparatus (Barnstead International, Dubuque, Iowa, USA).

*General Procedure for the Synthesis of Substituted Azido Benzene (**1a−d**).* The appropriate aniline derivative (1.0 equiv) was dissolved in a 10 mL mixture of conc. HCl and

https://doi.org/10.1021/acsomega.4c08385
ACS Omega 2025, 10, 6721−6734

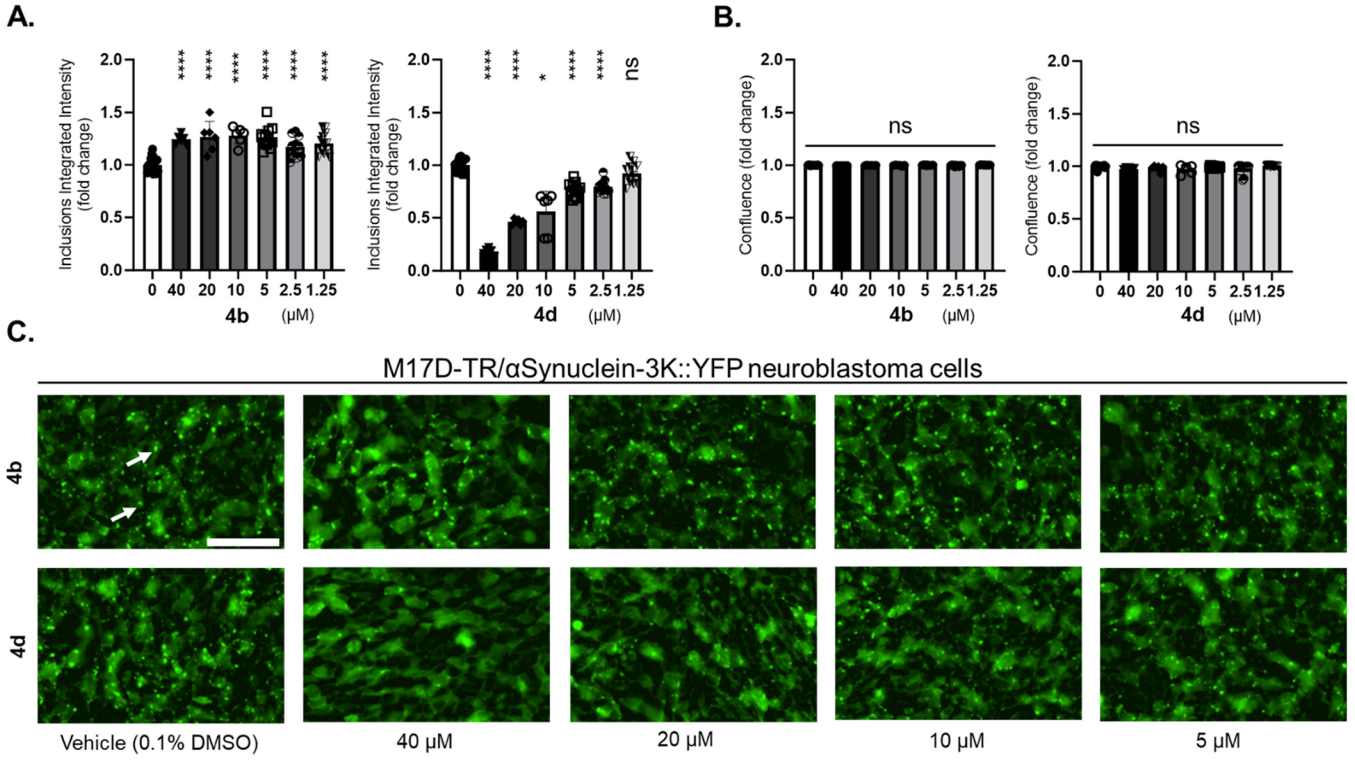

Figure 12. Formation of α-Syn inclusion was inhibited by **4d**. M17D cells expressing the inclusion-prone αS-3K::YFP fusion protein (dox-inducible) were treated with 0.1% DMSO (vehicle; "0 μM") as well as 1.25, 2.5, 5, 10, 20, and 40 μM of compounds **4b** and **4d** at t = 24 h after plating. αS-3K::YFP expression was induced with doxycycline at t = 48 h. (A) Incucyte-based analysis of punctate YFP signals relative to 0.1% DMSO was done at t = 96 h (N = 3 independent experiments, n = 6−18 individual wells total (0 μM, n = 18; 40, 20, and 10 μM, n = 6; 5, 2.5, and 1.25 μM n = 12). (B) Same as panel A, but confluence fold changes relative to DMSO vehicle (0 μM) were plotted. (C) Representative IncuCyte images of reporter cells treated with vehicle vs 40, 20, 10, and 5 μM compound 119 and 137 (t = 96 h), green channel. Arrows indicate αS-rich YFP-positive inclusions. Scale bar, 50 μm. All data are presented as fold-changes relative to DMSO control +/− standard deviation. One-way ANOVA, Dunnett's posthoc test; ∗, $p < 0.05$; ∗∗∗∗, $p < 0.0001$; ns, nonsignificant.

water (1:1) at 0−5 °C. Sodium nitrite (1.5 equiv) was gradually added over 5 min and the reaction mixture was stirred for 30 min. Sodium azide (2 equiv) was then added carefully, and the reaction mixture continuously stirred for 2−3 h. After completion, the mixture was extracted with dichloromethane (3 × 15 mL), filtered over anhydrous magnesium sulfate, and concentrated in vacuo to give the desired compounds. Some azides were needed for further purification using silica gel column chromatography (hexane/ethyl acetate 10:1 *v/v*) yielding the pure compounds in excellent yields (85−100%).

*1-Azido-4-methoxybenzene (**1a**).* 87% yield, white solid; ^{1}H NMR (500 MHz, $CDCl_3$) δ 6.96 (d, J = 9.0 Hz, 2H), 6.89 (d, J = 9.0 Hz, 2H), 3.79 (s, 3H). ^{13}C NMR (126 MHz, $CDCl_3$) δ 157.0, 132.3, 120.0, 115.1, 55.5.

*1-Azido-3,4-dimethoxybenzene (**1b**).* 92% yield, white solid; ^{1}H NMR (500 MHz, $CDCl_3$) δ 6.60 (d, J = 8.6 Hz, 1H), 6.35 (dd, J = 8.6, 2.6 Hz, 1H), 6.29 (d, J = 2.7 Hz, 1H), 3.63 (d, J = 2.7 Hz, 6H). ^{13}C NMR (126 MHz, $CDCl_3$) δ 149.9, 146.4, 132.5, 111.9, 110.2, 103.0, 55.8, 55.6.

*1-Azido-3,5-dimethoxybenzene (**1c**).* 96% yield, white solid; ^{1}H NMR (500 MHz, $CDCl_3$) δ 6.24 (t, J = 2.2 Hz, 1H), 6.17 (d, J = 2.3 Hz, 2H), 3.76 (s, 6H). ^{13}C NMR (126 MHz, CDCl3) δ 161.7, 141.9, 97.5, 97.2, 55.3.

*1-Azido-3,4,5-trimethoxybenzene (**1d**).* 100% yield, white solid; ^{1}H NMR (500 MHz, $CDCl_3$) δ 6.04 (s, 2H), 3.65 (s, 6H), 3.62 (s, 3H). ^{13}C NMR (126 MHz, $CDCl_3$) δ 153.9, 135.4, 96.2, 60.6, 55.8.

*1-Azido-4-dimethylamino Benzene (**1e**).* 97% yield, white solid; ^{1}H NMR (500 MHz, $CDCl_3$) δ 7.16−6.88 (m, 2H), 6.79 (s, 2H), 2.95 (s, 6H).

*1-Azido-4-chlorobenzene (**1f**).* 97% yield, pale gray solid; ^{1}H NMR (500 MHz, $CDCl_3$) δ 7.31 (d, J = 8.8 Hz, 2H), 6.96 (d, J = 8.8 Hz, 2H). ^{13}C NMR (126 MHz, $CDCl_3$) δ 138.7, 130.2, 129.9, 120.3.

*1-Azido-3,5-dichlorobenzene (**1g**).* 85% yield, white solid; ^{1}H NMR (500 MHz, $CDCl_3$) δ 7.10 (t, J = 1.8 Hz, 1H), 6.89 (d, J = 1.9 Hz, 2H). ^{13}C NMR (126 MHz, $CDCl_3$) δ 142.4, 136.0, 125.1, 117.7.

*1-Azido-4-nitrobenzene (**1h**).* 88% yield, white solid; ^{1}H NMR (500 MHz, DMSO) δ 8.19 (d, J = 9.1 Hz, 2H), 7.28 (d, J = 9.1 Hz, 2H). ^{13}C NMR (126 MHz, DMSO) δ 147.1, 144.5, 125.9, 120.5, 40.1, 39.9, 39.8.

*Synthesis of 5-Ethynyl-1H-indole (**2**).* 5-Iodo-1*H*-indole (1 equiv), bis(triphenylphosphine) palladium(II) dichloride (0.05 equiv), cuprous iodide (0.05 equiv), and triethyl amine (2 equiv) were added to DMF (2 mL) at room temperature under a N_2 atmosphere. Ethynyltrimethylsilane was slowly added, and the reaction was stirred for 5−8 h at room temperature. The reaction mixture was filtered through Celite pad and the organic layer was concentrated in vacuo. The residue was then treated with 0.2 M NaOH (2 mL) in methanol (5 mL) at room temperature for another 1 h. The reaction mixture was poured into water and extracted with ethyl acetate (3 × 20 mL), filtered over anhydrous magnesium sulfate, and concentrated. The desired compound was further

https://doi.org/10.1021/acsomega.4c08385
ACS Omega 2025, 10, 6721−6734

purified by column chromatography using hexane and ethyl acetate volume ratio of 5:1 (*v*/*v*).

*5-Ethynyl-1H-indole (**2**).* 72% yield, white solid; ^{1}H NMR (500 MHz, $CDCl_3$) δ 8.15 (s, 1H), 7.89 (dd, J = 1.6, 0.8 Hz, 1H), 7.37 (d, J = 1.6 Hz, 1H), 7.34−7.27 (m, 1H), 7.21−7.16 (m, 1H), 6.59−6.53 (m, 1H), 3.08 (s, 1H). ^{13}C NMR (126 MHz, $CDCl_3$) δ 135.7, 127.7, 126.0, 125.4, 125.4, 113.1, 111.3, 102.9, 85.5, 74.9.

*General Procedure for the Synthesis of 5-(1-(Substituted Phenyl)-1H-1,2,3-triazol-4-yl)-1H-indole and 4-(Benzo[b]-thiophen-5-yl)-1-(3,4,5-trimethoxyphenyl)-1H-1,2,3-triazole by Click Chemistry (**3a**−**3h**).* The azide derivative (1 equiv) and the acetylene derivative (e.g., **2**, 1.2 equiv) were dissolved in a mixture of THF and water (1:1) at room temperature. Then, sodium ascorbate (0.1 equiv) and copper sulfate (0.05 equiv) were added, and the reaction was stirred and followed by TLC. The reaction mixture was then partitioned between ethyl acetate and water. The organic layers were collected, dried over anhydrous magnesium sulfate, and concentrated under reduced pressure, The desired triazole was afforded by column chromatography using hexane/ethyl acetate at excellent yields.

*5-(1-(4-Methoxyphenyl)-1H-1,2,3-triazol-4-yl)-1H-indole (**3a**).* 84% yield, white solid; ^{1}H NMR (500 MHz, $CDCl_3$) δ 8.29 (s, 1H), 8.19 (dd, J = 1.6, 0.9 Hz, 1H), 8.10 (s, 1H), 7.77 (dd, J = 8.5, 1.6 Hz, 1H), 7.74−7.68 (m, 2H), 7.52−7.45 (m, 1H), 7.26 (d, J = 1.5 Hz, 1H), 7.08−7.02 (m, 2H), 6.65−6.59 (m, 1H), 3.88 (s, 3H). ^{13}C NMR (126 MHz, $CDCl_3$) δ 159.7, 149.6, 135.9, 130.8, 128.3, 125.0, 122.4, 122.2, 120.5, 118.3, 117.1, 114.8, 111.5, 103.1, 55.7.

*5-(1-(3,4-Dimethoxyphenyl)-1H-1,2,3-triazol-4-yl)-1H-indole (**3b**).* 83%, white solid; ^{1}H NMR (500 MHz, $CDCl_3$) δ 8.40 (s, 1H), 8.22−8.16 (m, 1H), 8.11 (s, 1H), 7.76 (dd, J = 8.4, 1.7 Hz, 1H), 7.47 (d, J = 8.4 Hz, 1H), 7.43 (d, J = 2.5 Hz, 1H), 7.26−7.21 (m, 2H), 6.97 (d, J = 8.6 Hz, 1H), 6.65−6.58 (m, 1H), 3.98 (s, 3H), 3.95 (s, 3H). ^{13}C NMR (126 MHz, $CDCl_3$) δ 149.8, 149.7, 149.3, 136.0, 130.9, 128.3, 125.2, 122.2, 120.4, 118.2, 117.3, 112.4, 111.6, 111.2, 105.0, 102.9, 56.24, 56.21.

*5-(1-(3,5-Dimethoxyphenyl)-1H-1,2,3-triazol-4-yl)-1H-indole (**3c**).* 91%, white solid; ^{1}H NMR (500 MHz, $CDCl_3$) δ 8.35 (s, 1H), 8.21−8.16 (m, 1H), 8.14 (s, 1H), 7.76 (dd, J = 8.4, 1.7 Hz, 1H), 7.47 (d, J = 8.4 Hz, 1H), 7.26−7.24 (m, 1H), 6.98 (d, J = 2.2 Hz, 2H), 6.64−6.59 (m, 1H), 6.52 (t, J = 2.2 Hz, 1H), 3.88 (s, 6H). ^{13}C NMR (126 MHz, $CDCl_3$) δ 161.5, 149.7, 138.8, 136.0, 128.3, 125.1, 122.1, 120.5, 118.3, 117.0, 111.6, 103.1, 100.4, 98.9, 55.8.

*5-(1-(3,4,5-Trimethoxyphenyl)-1H-1,2,3-triazol-4-yl)-1H-indole (**3d**).* 88% yield, white solid; ^{1}H NMR (500 MHz, $CDCl_3$) δ 8.42 (s, 1H), 8.19 (s, 1H), 8.13 (s, 1H), 7.76 (dd, J = 8.5, 1.7 Hz, 1H), 7.47 (d, J = 8.4 Hz, 1H), 7.26−7.24 (m, 1H), 7.02 (s, 2H), 6.65−6.57 (m, 1H), 3.95 (s, 6H), 3.91 (s, 3H). ^{13}C NMR (126 MHz, $CDCl_3$) δ 153.9, 149.7, 138.2, 136.0, 133.2, 128.3, 125.1, 122.1, 120.4, 118.3, 117.2, 111.6, 103.1, 98.5, 61.1, 56.5.

*5-(1-(4-Dimethylaminophenyl)-1H-1,2,3-triazol-4-yl)-1H-indole (**3e**).* 79% yield, white solid; ^{1}H NMR (500 MHz, $CDCl_3$) δ 8.25 (s, 1H), 8.19 (s, 1H), 8.08 (s, 1H), 7.77 (dd, J = 8.4, 1.6 Hz, 1H), 7.67 (d, J = 8.6 Hz, 2H), 7.48 (d, J = 8.5 Hz, 1H), 7.25 (s, 1H), 6.96 (s, 2H), 6.65−6.53 (m, 1H), 3.06 (s, 6H). ^{13}C NMR (126 MHz, $CDCl_3$) δ 144.4, 135.9, 131.2, 126.8, 126.4, 125.8, 125.0, 121.9, 120.6, 118.3, 117.0, 111.5, 103.2, 29.7.

*5-(1-(4-Chlorophenyl)-1H-1,2,3-triazol-4-yl)-1H-indole (**3f**).* 71% yield, pale gray solid, m.p.: 261.6−262.4 °C; ^{1}H NMR (500 MHz, DMSO) δ 11.22 (s, 1H), 9.21 (s, 1H), 8.13 (d, J = 1.7 Hz, 1H), 8.04−7.97 (m, 2H), 7.73−7.65 (m, 3H), 7.52−7.46 (m, 1H), 7.39 (t, J = 2.7 Hz, 1H), 6.55−6.45 (m, 1H). ^{13}C NMR (126 MHz, DMSO) δ 149.6, 136.4, 136.1, 133.2, 130.4, 128.4, 126.8, 121.9, 121.6, 119.6, 118.8, 117.6, 112.4, 102.0.

*5-(1-(3,5-Dichlorophenyl)-1H-1,2,3-triazol-4-yl)-1H-indole (**3g**).* 71% yield, white solid; ^{1}H NMR (500 MHz, $CDCl_3$) δ 8.32 (s, 1H), 8.22−8.15 (m, 1H), 8.14 (s, 1H), 7.80−7.67 (m, 2H), 7.58 (d, J = 1.9 Hz, 1H), 7.52−7.39 (m, 2H), 6.74 (d, J = 1.8 Hz, 1H), 6.66−6.57 (m, 1H). ^{13}C NMR (126 MHz, $CDCl_3$) δ 150.3, 138.5, 136.3, 136.0, 129.2, 128.4, 125.2, 123.8, 121.5, 120.4, 118.7, 118.5, 116.4, 111.6, 111.1, 103.2.

*5-(1-(4-Nitrophenyl)-1H-1,2,3-triazol-4-yl)-1H-indole (**3h**).* 75% yield, white solid; ^{1}H NMR (500 MHz, $CDCl_3$) δ 8.29 (s, 1H), 8.26−8.22 (m, 1H), 8.10−8.05 (m, 1H), 7.88 (d, J = 1.7 Hz, 1H), 7.63−7.57 (m, 2H), 7.43−7.33 (m, 2H), 6.97 (dd, J = 8.4, 1.8 Hz, 1H), 6.68−6.58 (m, 1H), 6.58−6.48 (m, 1H). ^{13}C NMR (126 MHz, $CDCl_3$) δ 135.8, 134.0, 126.4, 125.9, 125.3, 125.2, 124.8, 122.5, 121.7, 113.4, 112.0, 111.2, 103.3, 103.1.

*General Procedure for the Demethylation of (Poly)-Methoxy Derivatives (**4b**−**d**).* The methoxy substrate (1.00 equiv) was dissolved in DCM (5.0 mL) at room temperature and cooled to 0 °C on an ice bath. Boron tribromide (5.00 equiv. for each methoxy functionality) was added dropwise at 0 °C over 15 min. Then, the reaction mixture was stirred at 0 °C and allowed to warm to room temperature gradually overnight. Upon completion, the reaction was quenched with saturated NH_4Cl and extracted with ethyl acetate. The organic layer was dried with anhydrous magnesium sulfate and concentrated under a vacuum. The crude mixture was purified by column chromatography (DCM: methanol; 9:1 *v*/*v*).

*4-[4-(1H-Indol-5-yl)-1H-1,2,3-triazol-1-yl]benzene-1,2-diol (**4b**).* 8% yield; ^{1}H NMR (500 MHz, Acetone) δ 10.34 (s, 1H), 8.69 (s, 1H), 8.54 (s, 1H), 8.42 (s, 1H), 8.19 (d, J = 0.9 Hz, 1H), 7.76 (dd, J = 8.4, 1.6 Hz, 1H), 7.50 (d, J = 8.4 Hz, 1H), 7.46 (d, J = 2.6 Hz, 1H), 7.39−7.34 (m, 1H), 7.26 (dd, J = 8.5, 2.6 Hz, 1H), 7.01 (d, J = 8.5 Hz, 1H), 6.53 (ddd, J = 3.0, 1.9, 0.9 Hz, 1H). ^{13}C NMR (126 MHz, Acetone) δ 149.2, 145.9, 145.5, 136.3, 130.4, 128.5, 125.6, 122.4, 119.6, 117.4, 117.4, 115.6, 111.7, 111.6, 108.1, 101.9.

*5-[4-(1H-Indol-5-yl)-1H-1,2,3-triazol-1-yl]benzene-1,3-diol (**4c**).* 12% yield; ^{1}H NMR (500 MHz, MeOD) δ 8.63 (s, 1H), 8.09 (d, J = 0.9 Hz, 1H), 7.65 (dd, J = 8.4, 1.7 Hz, 1H), 7.52−7.41 (m, 1H), 7.27 (d, J = 3.2 Hz, 1H), 6.83 (dd, J = 4.5, 2.1 Hz, 2H), 6.51 (dd, J = 3.1, 0.9 Hz, 1H), 6.38 (t, J = 2.1 Hz, 1H). ^{13}C NMR (126 MHz, MeOD) δ 159.5, 149.7, 138.5, 136.5, 128.4, 125.3, 120.9, 119.2, 117.7, 117.5, 111.3, 102.4, 101.5, 98.7.

*5-[4-(1H-indol-5-yl)-1H-1,2,3-triazol-1-yl]benzene-1,2,3-triol (**4d**).* 9% yield; ^{1}H NMR (500 MHz, DMSO) δ 11.17 (s, 1H), 9.43 (s, 2H), 8.90 (s, 1H), 8.58 (s, 1H), 8.10 (s, 1H), 7.67 (dd, J = 8.4, 1.7 Hz, 1H), 7.45 (d, J = 8.4 Hz, 1H), 7.36 (d, J = 3.2 Hz, 1H), 6.84 (s, 2H), 6.47 (d, J = 3.1 Hz, 1H). ^{13}C NMR (126 MHz, DMSO) δ 149.0, 147.1, 136.3, 133.9, 128.9, 128.4, 126.6, 122.0, 119.6, 118.5, 117.5, 112.2, 101.9, 100.0.

Biophysical Experiments. *Chemical and Protein Source.* Heparin sodium salt was sourced from Millipore-Sigma, and Thioflavin T (ThT) used in the α-syn ThT assays was acquired from Alfa Aesar, Ward Hill, MA. Recombinant α-synuclein (α-

https://doi.org/10.1021/acsomega.4c08385
ACS Omega 2025, 10, 6721−6734

syn) and tau (2N4R) proteins were purchased from rPeptide (Watkinsville, GA).

The tau 0N4R protein was expressed and purified in the laboratory using established methods.[24] A plasmid containing the human Tau 0N4R isoform within the pET30a vector was generously provided by Dr. Benjamin Wolozin at Boston University. The plasmid was transformed into Rosetta BL21 *E. coli* cells (CamR), which were then grown in LB media containing 50 μg/mL kanamycin and 50 μg/mL chloramphenicol. Protein expression was triggered by the addition of 1 mM IPTG, followed by an incubation period of around 18 h at 37 °C. The bacterial cells were subsequently pelleted by centrifugation at 6000 g for 15 min at 4 °C. The cells were lysed in a buffer composed of 10 mM Hepes (pH 7.4), 50 mM NaCl, 1 mM MgCl2, 1 mM PMSF, 1× protease inhibitor cocktail, and 0.5 mM DTT. The cell mixture was then subjected to sonication, with 30-s pulses followed by 1 min pauses, at 30−45% power for a total of 5 min. After sonication, the lysate was centrifuged at 10,000 rpm for 10 min at 4 °C. The supernatant was then combined with 7.8 mL of 3 M NaCl and incubated in a water bath at 80 °C for 10 min, followed by a 10 min cooling period on ice. The solution was centrifuged again at 10,000 rpm for 10 min at 4 °C, and the supernatant was carefully transferred to new tubes. The supernatant was dialyzed overnight against a cation exchange buffer consisting of 50 mM MES, 1 M NaCl, 1 mM DTT, pH 6.0. Postdialysis, the sample was loaded onto a HiPrep SP HP column. Proteins were separated by applying a linear NaCl gradient from 50 mM to 1 M. The fractions containing the tau 0N4R isoform were pooled, dialyzed against PBS (pH 7.4). The resulting protein solution was stored at −80 °C.

The recombinant hyperphosphorylated tau (p-tau) isoform 1N4R was produced by the protein interaction module assisted function X (PIMAX) following the exact procedure published previously.[40,41] The construction was a generous gift from Dr. Min-Hao Kuo, Department of Biochemistry, Michigan State University.

Thioflavin T (ThT) Fluorescence Assays. The effects of the synthesized compounds on α-syn fibril formation were tested using a Thioflavin-T (ThT) fluorescence assay. The experiment was set up in a 96-well microplate. Compounds were added to each well to reach a final concentration of 100 μM, along with ThT, which was also at 100 μM. α-Syn (obtained from rPeptide) was then added to achieve a final concentration of 2 or 6 μM, using a stock solution of 277 μM dissolved in 20 mM Tris−HCl (pH 7.4). The assay buffer included 10 mM PBS (pH 7.4), 300 mM NaCl, 0.5 mM SDS, and a 3 mm borosilicate bead in each well. The plate was loaded into a Synergy HT multimode microplate reader (BioTek, Winooski, VT) and maintained at 37 °C. ThT fluorescence was monitored by measuring excitation at 440 nm and emission at 485 nm. Data were collected every 20 min, with the plate being shaken for 10 s before each reading. The fibril formation process was monitored for ≥37 h. Samples were tested in triplicate.

Thioflavin S (ThS) Fluorescence Assay. For the Thioflavin S (ThS) assay, a black 384-well flat-bottom microplate (Brand, ref 784076, medium binding) was employed. PBS (pH 7.4) from Gibco (catalog number 10010-023), treated with chelex beads (Biosciences, BTNM-0024), was added to each well to reach a final volume of 10 μL. The 2N4R tau peptide (obtained from rPeptide), 0N4R (recombinant protein produced in the laboratory), or p-tau (recombinant protein produced in the laboratory) was then introduced to achieve a final concentration of 6 or 12 μM, followed by the addition of DTT to 5 mM. The test compound was added to each well at a final concentration of 100 μM, and heparin was included at 150 μM. Arachidonic acid was then added to the mixture to reach a final concentration of 0.092 μg/mL (A0781, Fischer TCI). Thioflavin S (ThS) was incorporated at a final concentration of 40 μM to monitor fibril formation kinetics. Fluorescence intensity was recorded every 5 min, with a 30-s agitation step preceding each measurement.

Photo-Induced Cross-Linking of Unmodified Proteins (PICUP). Monomeric α-syn (obtained from rPeptide) and tau 0N4R (produced in the laboratory) were diluted to 30 and 6 μM in PBS (pH 7.4), respectively. Protein solutions were not incubated for any substantial time with the compounds prior PICUP. To initiate the cross-linking reaction, 2 μL of a 300 μM tris(bipyridine)ruthenium(II) complex solution and 2 μL of 6 mM ammonium persulfate were added to each tube. The PCR tubes were placed inside a dark enclosure. Control samples, which did not contain the $[Ru(bpy)_3]^{3+}$ complex, consisted of 0.25% DMSO. Light exposure was applied using a 53 W (120 V) incandescent bulb: α-syn was exposed for 1 s, and tau 0N4R was exposed for 15 s. After light exposure, 15% 2-mercaptoethanol was added to stop the free radicals. The samples were heated at 95 °C for 10 min on a heating block. The samples were then deposited into a 16% SDS-PAGE gel and, after electrophoresis, stained with Coomassie Blue. The final gels were scanned using the G:BOX F3 imaging system (Syngene). When necessary, high molecular weight band pixels were measured using ImageJ software.

Transmission Electron Microscopy. TEM analysis was carried out according to established protocols.[21−24,39] Tau isoform 2N4R (12 μM, purchased from rPeptide), along with the compounds of interest and control with 0.25% DMSO, was incubated in a reaction mixture containing 10 mM PBS (pH 7.4), 150 μM heparin, 5 mM dithiothreitol (DTT), and 10 mg/mL arachidonic acid for 5 days at 37 °C. For α-syn, the samples used in the ThT fibril formation assay were also analyzed by TEM. Concerning the disaggregation assays, a procedure previously published was followed using amyloid-β plaques isolated from AD brain and treated with different compounds at a concentration of 50 μM for 5 days at 37 °C prior to TEM analysis.[22] Protein determination was performed with the Lowry method using a bovine serum albumin (BSA) standard curve. For all different experiments, a small volume of sample (10 μL aliquot) was deposited on a 400-mesh Formvar-carbon-coated copper grid (Electron Microscopy Sciences, Hatfield, PA) and incubated for 1 min before being washed with distilled water. The grid was then air-dried, followed by a 1 min staining with 1% uranyl acetate. Grids were dried with filter paper prior to visualization with the JEOL 1400 Flash electron microscope (Japan) operating at 100 kV.

Quantitative measurement of the surface areas covered by fibrils and proto-fibrils in μm^2 was conducted to support the observed changes in density. The areas of eight different plaques for each sample were analyzed using ImageJ software. These measurements were then plotted and analyzed using GraphPad Prism 9, providing statistical validation of the surface area reduction after treatment. Statistical analyses consisted of the unpaired *t* test, two-tailed p value.

α-Synuclein Inclusion-Forming Neuroblastoma Cell Experiment. As in prior studies, doxycycline-inducible M17D-TR/αS-3K::YFP neuroblastoma cells were utilized to

https://doi.org/10.1021/acsomega.4c08385
ACS Omega 2025, 10, 6721−6734

assess the anti-inclusion effect of compounds.[21−24,37,39] For the assay, cells were initially seeded at 30,000 cells per well in 96-well plates. After a 24 h incubation period, compounds were added, and the αS-3K::YFP transgene expression was induced 24 h later by adding doxycycline to the media at a final concentration of 1 μg/mL. Continuous imaging of the cells was performed using the Incucyte Zoom 2000 system (Essen Biosciences), capturing both green fluorescence and bright field images. The assessment of inclusion formation and cell growth was conducted 48 h postinduction (96 h after initial plating). The Incucyte analysis settings for "Inclusions" were adjusted with a Fixed Threshold at 50 GCU, Edge Split with Sensitivity set to 100, and Cleanup parameters including Hole Fill set at 10 μm^2 and Adjust Size at 0 pixels. The filtering criteria included a maximum Area of 50 μm^2, a minimum Mean Intensity of 60, and a minimum Integrated Intensity of 2000. Cell confluence was measured using the 'Cells' processing settings with a Segmentation Adjustment of 0.7, Cleanup parameters set to 0, and Filters applying a minimum Area of 345 μm^2.

■ ASSOCIATED CONTENT

Data Availability Statement

The data underlying this study are available in the published article and its Supporting Information.

Supporting Information

The Supporting Information is available free of charge at https://pubs.acs.org/doi/10.1021/acsomega.4c08385.

Data pertaining to the characterization of compounds (NMR, HRMS, X-ray crystallographic data) and tau (0N4R) PICUP gels for quantification of monomers and oligomers (PDF)

■ AUTHOR INFORMATION

Corresponding Author

Jessica S. Fortin − *Department of Basic Medical Sciences, College of Veterinary Medicine, Purdue University, West Lafayette, Indiana 47907, United States;* orcid.org/0000-0002-1007-9360; Email: fortinj@purdue.edu

Authors

Ahmed A. Elbatrawy − *Department of Basic Medical Sciences, College of Veterinary Medicine, Purdue University, West Lafayette, Indiana 47907, United States;* orcid.org/0000-0001-6339-1190

Taiwo A. Ademoye − *Department of Basic Medical Sciences, College of Veterinary Medicine, Purdue University, West Lafayette, Indiana 47907, United States*

Heba Alnakhala − *Ann Romney Center for Neurologic Diseases, Department of Neurology, Brigham and Women's Hospital and Harvard Medical School, Boston, Massachusetts 02115, United States*

Arati Tripathi − *Ann Romney Center for Neurologic Diseases, Department of Neurology, Brigham and Women's Hospital and Harvard Medical School, Boston, Massachusetts 02115, United States*

Xiongwei Zhu − *Department of Pathology, Case Western Reserve University, Cleveland, Ohio 44106, United States*

Germán Plascencia-Villa − *Department of Neuroscience, Developmental and Regenerative Biology, The University of Texas at San Antonio, San Antonio, Texas 78249, United States*

George Perry − *Department of Neuroscience, Developmental and Regenerative Biology, The University of Texas at San Antonio, San Antonio, Texas 78249, United States;* orcid.org/0000-0002-6547-0172

Ulf Dettmer − *Ann Romney Center for Neurologic Diseases, Department of Neurology, Brigham and Women's Hospital and Harvard Medical School, Boston, Massachusetts 02115, United States*

Complete contact information is available at: https://pubs.acs.org/10.1021/acsomega.4c08385

Author Contributions

A.A.E. and T.A.A. contributed equally to this work. This project was conceived by J.S.F. Synthesis, characterization of compounds, data interpretation were performed by A.A.E. The ThT assays, cross-linking assays, and data interpretation were performed by T.A.A. and J.S.F. TEM and ThS experiments were performed by J.S.F. The cell culture experiments, statistics, and data interpretation were conducted by H.A., A.T., U.D. Amyloid plaques were secured by X.Z., G.P.-V., and G.P. Results were discussed with A.A.E., T.A.A., H.A., A.T., U.D., G.P.-V., G.P., J.S.F. The manuscript was drafted by A.A.E. and T.A.A. followed by editorial work from J.S.F. All authors contributed to this manuscript and approved the final version of this manuscript.

Funding

J.S.F. support was provided by the National Institutes of Health (NIH) grant (AG071985). G.P.-V. was supported by the Kleberg Foundation, Lowe Foundation, and Alzheimer's Association (AARFD-17-529742). U.D. was supported by NIH grants NS121826 and NS099328.

Notes

The authors declare no competing financial interest.

■ ACKNOWLEDGMENTS

The authors would like to acknowledge the assistance of Susantha K. Ganegamage for the demethylation procedure and the professional services of Alicia Withrow at the Center for Advanced Microscopy at Michigan State University. Constructs for tau 0N4R and p-tau 1N4R production were generous gift from Benjamin Wolozin (Boston University) and Min-Hao Kuo (Michigan State University), respectively.

■ ABBREVIATIONS

Aβ, amyloid-β; AD, Alzheimer's disease; DLB, dementia with Lewy bodies; dox, doxycycline; DTT, dithiothreitol; NFTs, neurofibrillary tangles; PD, Parkinson's disease; PICUPs, photoinduced cross-linking of unmodified proteins; SEM, standard error of the mean; α-syn, α-synuclein; TEM, transmission electron microscopy; ThT, thioflavin T; ThS, thioflavin S.

■ REFERENCES

(1) Irvine, G. B.; El-Agnaf, O. M.; Shankar, G. M.; Walsh, D. M. Protein aggregation in the brain: the molecular basis for Alzheimer's and Parkinson's diseases. *Mol. Med.* **2008**, *14* (7−8), 451−464.

(2) Peng, C.; Trojanowski, J. Q.; Lee, V. M. Protein transmission in neurodegenerative disease. *Nat. Rev. Neurol* **2020**, *16* (4), 199−212.

(3) Sweeney, P.; Park, H.; Baumann, M.; Dunlop, J.; Frydman, J.; Kopito, R.; McCampbell, A.; Leblanc, G.; Venkateswaran, A.; Nurmi, A.; et al. Protein misfolding in neurodegenerative diseases: implications and strategies. *Transl Neurodegener* **2017**, *6*, 6.

(4) Waddington-Cruz, M.; Ackermann, E. J.; Polydefkis, M.; Heitner, S. B.; Dyck, P. J.; Barroso, F. A.; Wang, A. K.; Berk, J. L.; Dyck, P. J. B.; Monia, B. P.; et al. Hereditary transthyretin amyloidosis: baseline characteristics of patients in the NEURO-TTR trial. *Amyloid* **2018**, *25* (3), 180−188.
(5) Price, J. L.; Morris, J. C. Tangles and plaques in nondemented aging and "preclinical" Alzheimer's disease. *Ann. Neurol.* **1999**, *45* (3), 358−368.
(6) Rajmohan, R.; Reddy, P. H. Amyloid-Beta and Phosphorylated Tau Accumulations Cause Abnormalities at Synapses of Alzheimer's disease Neurons. *J. Alzheimers Dis* **2017**, *57* (4), 975−999.
(7) Gulisano, W.; Maugeri, D.; Baltrons, M. A.; Fa, M.; Amato, A.; Palmeri, A.; D'Adamio, L.; Grassi, C.; Devanand, D. P.; Honig, L. S.; et al. Role of Amyloid-beta and Tau Proteins in Alzheimer's Disease: Confuting the Amyloid Cascade. *J. Alzheimers Dis* **2018**, *64* (s1), S611−S631.
(8) Buxbaum, J. N.; Dispenzieri, A.; Eisenberg, D. S.; Fandrich, M.; Merlini, G.; Saraiva, M. J. M.; Sekijima, Y.; Westermark, P. Amyloid nomenclature 2022: update, novel proteins, and recommendations by the International Society of Amyloidosis (ISA) Nomenclature Committee. *Amyloid* **2022**, *29* (4), 213−219.
(9) Metaxas, A.; Kempf, S. J. Neurofibrillary tangles in Alzheimer's disease: elucidation of the molecular mechanism by immunohisto-chemistry and tau protein phospho-proteomics. *Neural Regen Res.* **2016**, *11* (10), 1579−1581.
(10) Braak, H.; Alafuzoff, I.; Arzberger, T.; Kretzschmar, H.; Del Tredici, K. Staging of Alzheimer disease-associated neurofibrillary pathology using paraffin sections and immunocytochemistry. *Acta Neuropathol* **2006**, *112* (4), 389−404.
(11) Rawat, P.; Sehar, U.; Bisht, J.; Selman, A.; Culberson, J.; Reddy, P. H. Phosphorylated Tau in Alzheimer's Disease and Other Tauopathies. *Int. J. Mol. Sci.* **2022**, *23* (21), No. 12841.
(12) Mietelska-Porowska, A.; Wasik, U.; Goras, M.; Filipek, A.; Niewiadomska, G. Tau protein modifications and interactions: their role in function and dysfunction. *Int. J. Mol. Sci.* **2014**, *15* (3), 4671−4713.
(13) Diociaiuti, M.; Bonanni, R.; Cariati, I.; Frank, C.; D'Arcangelo, G. Amyloid Prefibrillar Oligomers: The Surprising Commonalities in Their Structure and Activity. *Int. J. Mol. Sci.* **2021**, *22* (12), 6435.
(14) Mandelkow, E. M.; Mandelkow, E. Biochemistry and cell biology of tau protein in neurofibrillary degeneration. *Cold Spring Harb Perspect Med.* **2012**, *2* (7), No. a006247.
(15) Serrano-Pozo, A.; Frosch, M. P.; Masliah, E.; Hyman, B. T. Neuropathological alterations in Alzheimer disease. *Cold Spring Harb Perspect Med.* **2011**, *1* (1), No. a006189.
(16) Ohm, D. T.; Fought, A. J.; Martersteck, A.; Coventry, C.; Sridhar, J.; Gefen, T.; Weintraub, S.; Bigio, E.; Mesulam, M. M.; Rogalski, E.; et al. Accumulation of neurofibrillary tangles and activated microglia is associated with lower neuron densities in the aphasic variant of Alzheimer's disease. *Brain Pathol* **2021**, *31* (1), 189−204.
(17) Wakabayashi, K.; Tanji, K.; Mori, F.; Takahashi, H. The Lewy body in Parkinson's disease: molecules implicated in the formation and degradation of alpha-synuclein aggregates. *Neuropathology* **2007**, *27* (5), 494−506.
(18) Manzanza, N. O.; Sedlackova, L.; Kalaria, R. N. Alpha-Synuclein Post-translational Modifications: Implications for Patho-genesis of Lewy Body Disorders. *Front Aging Neurosci* **2021**, *13*, No. 690293.
(19) Zamel, J.; Chen, J.; Zaer, S.; Harris, P. D.; Drori, P.; Lebendiker, M.; Kalisman, N.; Dokholyan, N. V.; Lerner, E. Structural and dynamic insights into alpha-synuclein dimer conformations. *Structure* **2023**, *31* (4), 411−423 e416.
(20) Saramowicz, K.; Siwecka, N.; Galita, G.; Kucharska-Lusina, A.; Rozpedek-Kaminska, W.; Majsterek, I. Alpha-Synuclein Contribution to Neuronal and Glial Damage in Parkinson's Disease. *Int. J. Mol. Sci.* **2024**, *25* (1), 360.
(21) Ramirez, E.; Ganegamage, S. K.; Elbatrawy, A. A.; Alnakhala, H.; Shimanaka, K.; Tripathi, A.; Min, S.; Rochet, J. C.; Dettmer, U.; Fortin, J. S. 5-Nitro-1,2-benzothiazol-3-amine and N-Ethyl-1-[(ethylcarbamoyl)(5-nitro-1,2-benzothiazol-3-yl)amino]formamide Modulate alpha-Synuclein and Tau Aggregation. *ACS Omega* **2023**, *8* (22), 20102−20115.
(22) Ramirez, E.; Ganegamage, S. K.; Min, S.; Patel, H.; Ogunware, A.; Plascencia-Villa, G.; Alnakhala, H.; Shimanaka, K.; Tripathi, A.; Wang, K. W.; et al. Evaluation of N- and O-Linked Indole Triazines for a Dual Effect on alpha-Synuclein and Tau Aggregation. *ACS Chem. Neurosci.* **2023**, *14* (21), 3913−3927.
(23) Ramirez, E.; Min, S.; Ganegamage, S. K.; Shimanaka, K.; Sosa, M. G.; Dettmer, U.; Rochet, J. C.; Fortin, J. S. Discovery of 4-aminoindole carboxamide derivatives to curtail alpha-synuclein and tau isoform 2N4R oligomer formation. *Results Chem.* **2023**, *5*, No. 100938.
(24) Elbatrawy, A. A.; Ademoye, T. A.; Alnakhala, H.; Tripathi, A.; Zami, A.; Ostafe, R.; Dettmer, U.; Fortin, J. S. Discovery of small molecule benzothiazole and indole derivatives tackling tau 2N4R and alpha-synuclein fibrils. *Bioorg. Med. Chem.* **2024**, *100*, No. 117613.
(25) Dheer, D.; Singh, V.; Shankar, R. Medicinal attributes of 1,2,3-triazoles: Current developments. *Bioorg Chem.* **2017**, *71*, 30−54.
(26) Qu, W.; Kung, M. P.; Hou, C.; Oya, S.; Kung, H. F. Quick assembly of 1,4-diphenyltriazoles as probes targeting beta-amyloid aggregates in Alzheimer's disease. *J. Med. Chem.* **2007**, *50* (14), 3380−3387.
(27) Das, S.; Smid, S. D. Identification of dibenzyl imidazolidine and triazole acetamide derivatives through virtual screening targeting amyloid beta aggregation and neurotoxicity in PC12 cells. *Eur. J. Med. Chem.* **2017**, *130*, 354−364.
(28) Bieschke, J.; Russ, J.; Friedrich, R. P.; Ehrnhoefer, D. E.; Wobst, H.; Neugebauer, K.; Wanker, E. E. EGCG remodels mature alpha-synuclein and amyloid-beta fibrils and reduces cellular toxicity. *Proc. Natl. Acad. Sci. U. S. A.* **2010**, *107* (17), 7710−7715.
(29) Sonawane, S. K.; Chidambaram, H.; Boral, D.; Gorantla, N. V.; Balmik, A. A.; Dangi, A.; Ramasamy, S.; Marelli, U. K.; Chinnathambi, S. EGCG impedes human Tau aggregation and interacts with Tau. *Sci. Rep* **2020**, *10* (1), 12579.
(30) Yang, Z.; Yao, Y.; Zhou, Y.; Li, X.; Tang, Y.; Wei, G. EGCG attenuates alpha-synuclein protofibril-membrane interactions and disrupts the protofibril. *Int. J. Biol. Macromol.* **2023**, *230*, No. 123194.
(31) Goncalves, P. B.; Sodero, A. C. R.; Cordeiro, Y. Green Tea Epigallocatechin-3-gallate (EGCG) Targeting Protein Misfolding in Drug Discovery for Neurodegenerative Diseases. *Biomolecules* **2021**, *11* (5), 767.
(32) Martins, G. F.; Nascimento, C.; Galamba, N. Mechanistic Insights into Polyphenols' Aggregation Inhibition of alpha-Synuclein and Related Peptides. *ACS Chem. Neurosci.* **2023**, *14* (10), 1905−1920.
(33) Biancalana, M.; Makabe, K.; Koide, A.; Koide, S. Molecular mechanism of thioflavin-T binding to the surface of beta-rich peptide self-assemblies. *J. Mol. Biol.* **2009**, *385* (4), 1052−1063.
(34) Rinauro, D. J.; Chiti, F.; Vendruscolo, M.; Limbocker, R. Misfolded protein oligomers: mechanisms of formation, cytotoxic effects, and pharmacological approaches against protein misfolding diseases. *Mol. Neurodegener* **2024**, *19* (1), 20.
(35) Wells, C.; Brennan, S.; Keon, M.; Ooi, L. The role of amyloid oligomers in neurodegenerative pathologies. *Int. J. Biol. Macromol.* **2021**, *181*, 582−604.
(36) Yao, Y.; Tang, Y.; Wei, G. Epigallocatechin Gallate Destabilizes alpha-Synuclein Fibril by Disrupting the E46-K80 Salt-Bridge and Inter-protofibril Interface. *ACS Chem. Neurosci.* **2020**, *11* (24), 4351−4361.
(37) Terry-Kantor, E.; Tripathi, A.; Imberdis, T.; LaVoie, Z. M.; Ho, G. P. H.; Selkoe, D.; Fanning, S.; Ramalingam, N.; Dettmer, U. Rapid Alpha-Synuclein Toxicity in a Neural Cell Model and Its Rescue by a Stearoyl-CoA Desaturase Inhibitor. *Int. J. Mol. Sci.* **2020**, *21* (15), 5193.
(38) Imberdis, T.; Negri, J.; Ramalingam, N.; Terry-Kantor, E.; Ho, G. P. H.; Fanning, S.; Stirtz, G.; Kim, T. E.; Levy, O. A.; Young-Pearse, T. L.; et al. Cell models of lipid-rich alpha-synuclein

https://doi.org/10.1021/acsomega.4c08385
ACS Omega 2025, 10, 6721−6734

aggregation validate known modifiers of alpha-synuclein biology and identify stearoyl-CoA desaturase. *Proc. Natl. Acad. Sci. U. S. A.* **2019**, *116* (41), 20760−20769.
(39) Fortin, J. S.; Shimanaka, K.; Saraswati, A. P.; Liu, M.; Wang, K. W.; Hagar, H. T.; Maity, S.; Ganegamage, S. K.; Ellsworth, E.; Counts, S. E.; et al. Anti-fibrillization effects of sulfonamide derivatives on alpha-synuclein and hyperphosphorylated tau isoform 1N4R. *J. Mol. Struct.* **2022**, *1267*, No. 133574.
(40) Sui, D.; Xu, X.; Ye, X.; Liu, M.; Mianecki, M.; Rattanasinchai, C.; Buehl, C.; Deng, X.; Kuo, M. H. Protein interaction module-assisted function X (PIMAX) approach to producing challenging proteins including hyperphosphorylated tau and active CDK5/p25 kinase complex. *Mol. Cell Proteomics* **2015**, *14* (1), 251−262.
(41) Liu, M.; Dexheimer, T.; Sui, D.; Hovde, S.; Deng, X.; Kwok, R.; Bochar, D. A.; Kuo, M. H. Hyperphosphorylated tau aggregation and cytotoxicity modulators screen identified prescription drugs linked to Alzheimer's disease and cognitive functions. *Sci. Rep* **2020**, *10* (1), 16551.

https://doi.org/10.1021/acsomega.4c08385
ACS Omega 2025, 10, 6721−6734